A field study on ice melting and breakup in a boreal lake, Pääjärvi, in Finland

Yaodan Zhang[1,2], Marta Fregona[3], John Loehr[2], Joonatan Ala-Könni[4], Shuang Song[5,6], Matti Leppäranta[4], and Zhijun Li[1]

[1]State Key Laboratory of Coastal and Offshore Engineering, Dalian University of Technology, Dalian, China
[2]Lammi Biological Station, University of Helsinki, Finland
[3]Department of Civil, Environmental and Mechanical Engineering, University of Trento, Trento, Italy
[4]Institute of Atmospheric and Earth Sciences, University of Helsinki, Helsinki, Finland
[5]Water Conservancy and Civil Engineering College, Inner-Mongolia Agricultural University, Hohhot, China
[6]College of Water Conservancy, Shenyang Agricultural University, Shenyang, China

Correspondence to: Zhijun Li (lizhijun@dlut.edu.cn), Yaodan Zhang (zhangyaodan@mail.dlut.edu.cn).

Abstract. Lake ice melting and breakup form a fast, nonlinear process with important mechanical, chemical, and biological consequences. The process is difficult to study in the field due to safety issues, and therefore only little is known about its details. In the present work, the field data were collected on foot, by hydrocopter, and by boat for a full time-series of the evolution of ice thickness, structure, and geochemistry through the melting period. The observations were made in Lake Pääjärvi in 2018 (pilot study) and 2022. In 2022, the maximum thickness of ice was 55 cm with 60 % snow-ice, and in 40 days the ice melted by 33 cm from the surface and 22 cm from the bottom while the porosity increased from less than 5% to 40−50 % at breakup. In 2018, the snow-ice layer was thin, and bottom and internal melting dominated the ice decay. The mean melting rates were 1.31 cm d^{-1} in 2022 and 1.55 cm d^{-1} in 2018. In 2022 the electrical conductivity (EC) of ice was 11.4 ± 5.79 μS cm^{-1}, one order of magnitude lower than in the lake water, and ice pH was 6.44 ± 0.28, lower by 0.4 than in water. The pH and EC of ice and water decreased along the ice decay except for slight increases in ice due to flushing by lake water. Chlorophyll *a* was less than 0.5 μg L^{-1} in porous ice, approximately one-third of that in the lake water. The results are important for understanding the process of ice decay with consequences to lake ecology, further development of numerical lake ice models, and modeling the safety of ice cover and ice loads.

1 Introduction

Lake ice is a thin layer between the atmosphere and lake water body and plays an important role in the local environment and human life (Leppäranta, 2015). Lake ice affects the local weather by altering the heat, mass and momentum exchange between the atmosphere and lake water body, as seen in the surface

caused by the heat flux from water that can be large in spring due to the solar heating of the under-ice water (Jakkila et al., 2009; Shirasawa et al., 2006).

We examine here the decay of ice in a boreal lake, Lake Pääjärvi, in southern Finland by field surveys in two years, 2018 and 2022. The objective was to analyse the ice melting process for the evolution of ice thickness and porosity as well as for the changes in ice and water geochemistry. The structure and properties of ice experienced remarkable changes during the decay process, and significant melting occurred in the surface and bottom and in the interior. Flushing of ice by meltwater and lake water caused changes to ice and water geochemistry. A deeper knowledge of the ice decay is needed for modelling the lake ice decay, particularly for ice engineering issues, and for understanding the physical and geochemical conditions for ecology of freezing lakes in spring. This paper gives the results of the Lake Pääjärvi field program.

2 Materials and methods

2.1 Study site

Lake Pääjärvi is located in the boreal zone in southern Finland (61°40′ N, 25°08′ E). The lake area is 13.4 km^2, the mean and maximum depths are 14.4 m and 87 m, respectively, and the catchment area is 244 km^2 (Arvola et al., 1996). Lake Pääjärvi is a humic, brown-water lake with an average optical depth of 0.67 m and Secchi depth of 1.8 m (Arst et al., 2008). The decay of the ice cover takes about one month, controlled by the presence of snow on top, the optical quality of snow and ice, and the atmospheric and solar forcing (Wang et al., 2005; Jakkila et al., 2009). The LBS ice phenology data base shows that in 1970–2022 the ice breakup date was on average April 25, with a standard deviation of 12 days. In 1993–1999, the maximum annual ice thickness was on average 46 cm with the standard deviation of 12 cm, and the fraction of snow-ice was on average one-third (Leppäranta and Kosloff, 2000).

The field study was made in Pappilanlahti Bay in the west side of the lake near the Lammi Biological Station (LBS). The bay is shallow (maximum depth 12 m), with three small inflow brooks and a weak groundwater flux at the bottom. The field site was about 100 m from the shore with access

first by foot and in late season by a hydrocopter and a boat. Our field program included a pilot study in 12–20 April 2018 and the main experiment in 25 March – 3 May 2022, which was more extensive and provided the main body of the data. The ice situation was recorded by ground photographs, drone orthophotos, and field notes, and ice and water samples were collected at regular field visits. In 2022 the whole decay period was mapped while in 2018 just the last eight days of it.

2.2 Observations

In the pilot study in 2018, the field site was visited five times between April 12 and April 20. The study was focused on a short period at the end of the ice decay. Ice samples were taken on April 12, 15 and 20, and thereafter, because of the rapid melting, it was not possible to walk on the ice or to use a boat for sampling, but photographs were taken daily from the shore. Analyses of samples were made in similar manner as in the main experiment (see below).

The study period in 2022 covered the whole decay period from March 25 to May 3 with eight field site visits. The sampling was made by foot from the shore until April 22. Then an open water zone formed at the shoreline, and a hydrocopter was used for ice sampling on April 26–29 (Fig. 1a). On May 3, the melting created several open channels, and a boat was used for the sampling. Each time the quality and thickness of ice were recorded first with the freeboard, snow thickness, snow-ice thickness, and congelation ice thickness measured by a ruler. Ice samples (cross-section 30 cm × 30 cm) were cut by drill and saw, put in plastic bags, and transported immediately to a freezer (temperature –18 °C) in LBS. Water samples were taken from the drill holes and stored in sealed bottles in a fridge at a temperature of 4–6 °C.

Figure 1. Lake ice sampling and processing: (a) collect ice with a handsaw on the hydrocopter; (b) the ice block was sliced into four parts for different observations.

Available routine meteorological and hydrological data of the Finnish Meteorological Institute (FMI) and Finnish Environment Institute (SYKE) were utilized. The SYKE data include manual measurements of the thicknesses of ice, snow-ice and snow, and freeboard every ten days during the whole winter in Pappilanlahti Bay, and they were used for the all-season ice and snow thickness reference and control. FMI provided the meteorological data of an automated station in LBS yard half a kilometre from our lake site and solar radiation data for the closest radiation site in Jokioinen. The LBS data base was utilized for the long-term ice phenology and geochemistry of the lake and inflow brooks of the study bay.

2.3 Laboratory work

The ice samples were analysed in the INAR (Institute of Atmospheric and Earth Sciences, University of Helsinki) ice laboratory (-10 °C). Each ice sample was divided into four sections. Section 1 was cut vertically into layers for the geochemistry analyses from meltwater in the water laboratory. Section 2 was cut vertically and horizontally to map the ice crystal structure and study the gas bubbles by image analysis, and Section 3 was cut vertically to layers to measure the density of ice. Section 4 was stored as a backup (Fig. 1b).

The samples were cut into vertical sections of $8-10$ cm height by a bandsaw, and horizontal sections were extracted at the vertical cuts. The size and distribution of gas bubbles in the ice were

observed under normal light (Deng et al., 2019). The sections were frozen on glass plates to be prepared for thin sections, and the crystal structure of ice was obtained from the thin sections between crossed polarizers (Langway, 1959). The mass/volume method was used to measure the ice density in the laboratory, and the freeboard in the field was used as a control. The sample was cut into 5 cm cuboids by a bandsaw. The sides of a cuboid were measured by a vernier caliper, and the mass was measured by an electronic scale with the accuracy of 0.001 g. The accuracy of the density is estimated as 10 kg m^{-3} determined by the accuracy of the volume measurement.

The water samples as well as the ice meltwater samples were analysed in the LBS water laboratory for pH, electrical conductivity (EC) and chlorophyll *a* (Chl *a*). The ice geochemistry samples were first cut in the ice laboratory into vertical sections based on the structure at intervals of 8 – 10 cm by a bandsaw, melted in sealed bags, poured into sample bottles, and stored in a fridge (at 4–6 °C). pH and EC were measured from unfiltered samples according to the standards in SFS-EN 27888 and SFS 3021 using a Thermo Orion 3-STAR Precision Benchtop pH meter (accuracy 0.01) and YSI 3200 conductivity sensor (accuracy 0.01 μS cm^{-1}). The Chl *a* concentration was measured from the light absorbance at 665 and 750 nm wavelengths (Arvola et al. 2014).

3 Results

3.1 Ice structure

3.1.1 Ice structure in the pilot study 2018

In 2018, the ice decay period began at the end of March, and the final breakup took place on April 25. The thickness of ice was 42 cm on March 30, and on April 12 it was 35 cm with 5.3 cm snow-ice and 29.7 cm congelation ice (Table 1). Snow-ice melted in less than eight days, and congelation ice melted fast after April 15. On April 24, rain greatly accelerated the melting.

Table 1. Thickness of ice layers and freeboard in the melting phase (cm) and porosity (%) in April 2018, also shown is the ratio of freeboard (Fb) to draft.

2018	Snow-ice	Congelation ice	Total ice	Porosity	Freeboard	Fb/draft
April 12	5.3	29.7	35.0	~ 0	3.0	0.094
April 13	4.7	29.3	34.0	x	3.0	0.097
April 14	3.3	28.7	32.0	x	2.0	0.067

April 15	2.7	28.3	31.0	x	2.0	0.069
April 20	0	20.3	20.3	25	x	x
April 25	0	0	0	x	0	x

3.1.2 Ice structure in the main experiment 2022

The ice decay period began on March 25 and the final breakup took place after 42 days on May 5 (Table 2). The thickness of ice was 55 cm on March 25, close to the long-term mean, with 33 cm congelation ice and 22 cm snow-ice. During the decay period the ice was melting at both boundaries and in the interior. At the end of April there was a slush layer between the surface ice layer and the congelation ice layer with soft places so that walking on the ice was not easy.

Table 2. Thickness of ice layers and freeboard in the melting phase (cm) and porosity (%) in 2022, also shown is the ratio of freeboard (Fb) to draft. x stands for no data.

2022	Snow-ice	Congelation ice	Total ice	Porosity	Freeboard	Fb/draft	Snow
March 25	33	22	55	x	5.5	0.11	1
April 1	31	20	51	6.1	5	0.11	2.5
April 8	30	17	47	x	2	0.044	13
April 14	31	17	48	7.7	5	0.12	2
April 22	27	11	38	15.2	4	0.12	0
April 26	7.5 + 7¶	10	24.5	17.1	1	0.043	0
April 29	6 + 12¶	4	22	24.1	0.5	0.023	0
May 3	2	0	2	34.0	x	x	0
May 5	0	0	0	x	0	x	0

¶ Surface ice + slush layer

Figure 2 shows drone orthophotos of the ice cover taken at an altitude of 100 m during the melting period. As reported by Ashton (1985) about melting lake ice in general, the ice cover of Lake Pääjärvi looked grayish and patchy from above. Snowfall turned the ice white at the beginning of April, and as the air temperature increased, the new snow began to melt creating a patchy surface. The positive al

Figure 2. Drone orthophotos of the ice cover in the melting period in 2022 (time given as month.day).

There were two principle vertical layers in the Lake Pääjärvi ice cover (Fig. 3). The top layer was granular snow-ice, with the grain size of 1–9 mm and blurred crystal boundaries, and the lower layer was clear columnar congelation ice with the grain size of 2–10 cm. When the ice melting progressed, the ice crystal structure data showed that the thickness of both snow-ice and congelation ice decreased, and the porosity of ice increased.

The ice melted 4 cm in May 25–April 1. On April 1, the snow-ice part had two sub-layers (Fig. 3). The top 27 cm sub-layer had very irregular crystal structure with blurred crystal boundaries and grain size mainly within 1 – 2 mm. In the lower, 27 – 31 cm, layer the crystals were granular with clear boundaries, and the grain size was mainly 2 – 5 mm. It was judged that the upper sub-layer had undergone thawing and refreezing process. The columnar ice layer underneath was clear ice with grain size increasing with depth, from 2 to 10 cm. The volume fraction of gas bubbles was 4 – 6 % in the snow-ice layer. They were cylindrical and spherical shaped with the maximum diameter of 4 mm. The corresponding fraction was 1 – 2 % in congelation ice, the bubbles were spherical with the maximum diameter of 1 mm.

In April 1–14 congelation ice melted by 3 cm, but snow-ice thickness was unchanged. According to the weather data, a snowfall began on April 5, and then the air temperature rose resulting in the formation of new snow-ice through the melt–freeze cycle. Compared with April 1, the ice crystal size had not changed, and the gas volume of snow-ice was 5 – 7 %. After April 14, the air temperature increased further, and the ice melted by 10 cm in April 14 – 22. The horizontal and vertical sections showed strong melting at the grain boundaries in snow-ice (Fig. 4a). The gas content increased in snow-ice to 6 – 10 % and in congelation ice to 1 – 3 %. Also, the maximum diameter of gas bubbles increased to 5 mm in snow-ice and 3 mm in congelation ice.

In April 26–29, a slush layer appeared below a surface ice layer due to internal melting of ice (Fig. 4b). The columnar ice began to melt at crystal boundaries where gas inclusions appeared. On April 29, the gas volume reached 5 % in the columnar layer, with the maximum bubble size equal to 5 mm. On May 3, the columnar ice and slush layers had melted, and there was only 2 cm snow-ice left (Fig. 4c).

Figure 3. Lake Pääjärvi ice crystal structure of April 1. (a) vertical profiles under the normal light (left) and ice crystal structure under the polarized light (right), (b) horizontal sections under the normal light (top) and ice crystal structure under the polarized light (bottom).

Figure 4. Lake Pääjärvi ice crystal structure of April 22, April 26, and May 3. (a) vertical profiles under the normal light (left) and ice crystal structure under the polarized light (right) on April 22; (b) vertical profiles under the normal light (left) and ice crystal structure under the polarized light (right) on April 26; (c) vertical profiles under the normal light (left) and ice crystal structure under the polarized light (right) on May 3.

3.1.3 Ice melt rate

The ice sample data in Tables 1–2 were used to estimate the melting at the surface and bottom and in the ice interior. The melting rate increased toward the breakup date. In 2018 the ice cover was different from 2022 in that the ice was mostly (85 %) congelation ice (Table 1). In April 12−20 the mean surface and bottom melting together was 1.84 cm d^{-1}, and the mean internal melting was 0.86 cm d^{-1}. In April 12–15 the mean surface and bottom melting were 0.87 cm d^{-1} and 0.47 cm d^{-1}, respectively. The ice was more transparent than in 2022 that allowed more sunlight penetration through ice. The bottom melting in 12–15 April corresponded to the heat flux

$$Q = \frac{\rho_i L_f \Delta h}{\Delta t} = 16 \text{ W m}^{-2} \quad (1)$$

where ρ_i is ice density, L_f is the latent heat of freezing, Δh is the change in ice thickness, and $\Delta t =$ 1 d.

Table 3. Ice melting in spring 2018 (cm). The numbers show the change from the row above to the present one. At the end, surface melting and bottom melting cannot be separated from the data as shown by z1 and z2. x is for no data.

2018	Surface melt	Bottom melt	Total melt	Internal melt
April 12	0	0	0	0
April 13	0.6	0.4	1.0	x
April 14	1.4	0.6	2.0	x
April 15	0.6	0.4	1.0	x
April 20	2.7+ z1	8.0 – z1	10.7	6.9
April 25	z2	20.3–z2	20.3	x

In 2022 the mean rate was 1.31 cm d^{-1}, and snow-ice melted a little faster than congelation ice. The mean melt rates were, respectively, 0.79 cm d^{-1} and 0.38 cm d^{-1}. There was a minor new snow-ice formation on April 14, and the last 2 cm thick piece was snow-ice on May 3. The mean melt rate at the bottom corresponds to the heat flux of 13 W m^{-2} from water to ice. This flux was larger than normally assumed (e.g., Yang et al., 2012). The mean internal melt rate was 0.18 cm d^{-1} equivalent ice thickness that was smaller than the surface and bottom melting, attributed to the low light transmittance of snow-ice. In the last week of melting, the ice was highly porous and internal breakages occurred.

Table 4. Ice melting in spring 2022 (cm). The numbers show the change from the row above to the present one.

2022	Surface melt	Bottom melt	Total melt	Internal melt
March 25	0	0	0	0
April 1	2	2	4	x
April 8	1	3	4	0.4
April 14	-1	0	-1	0.4
April 22	4	6	10	3.2
April 26	4.5	1	5.5	0.6
April 29	4.5	6	10.5	1.6
May 3	16	4	20	1.2
May 5	2	0	2	0
Sum	33	22	55	7.4

3.2 Ice density

At the initial stage of melting, April 1 – 14, 2022, the estimated average densities of snow-ice and congelation ice were 850 kg m^{-3} and 930 kg m^{-3}, respectively. The congelation ice data are from the deep layers, and the apparently high density is likely due to liquid water in pores. The density profiles shifted toward lower level with time while the density always increased with depth (Fig. 5). On April 22

the snow-ice density was higher than on April 14 at large depth that can be due to meltwater accumulation in deep pores. Toward the ice breakup, the density decreased, in snow-ice to below 700 kg m^{-3} and in congelation ice to almost 700 kg m^{-3}. The density data were used to estimate the porosity, which was found to increase from 6.1 % to 34 % during the melting period (Table 2).

Figure 5. Lake Pääjärvi ice density profiles in 2022 (asterisk stands for

returning to ice bottom. Eq. (5) gives the part of solar radiation used for internal melting, and the bottom melting in Eq. (6) consists of the background heat flux from the deep water (Q_{w0}) and a part of the under-ice solar radiation.

The heat fluxes for ice melting in 2022 were estimated from Eqs. (4-6). The forcing was provided by the solar radiation data of FMI station Jokioinen and by the air temperature data of FMI station Lammi. It was assumed that the surface temperature was at the melting point. The incident solar radiation averaged to 126 W m^{-2} in the last week of March and 198 W m^{-2} in the first week of May, and the maximum daily average was 268 W m^{-2}, on April 25. The albedo was parameterized as $\alpha = 0.7$ for snow, 0.5 for dry ice and 0.3 for wet ice, and $\lambda = 0.5$ m^{-1} was fixed. The mean solar radiation and the mean air temperature were 184 W m^{-2} and 2.4 °C in April 2022, while the corresponding climatological values are 152 W m^{-2} and 3.5 °C.

The function k_0 was estimated based on Leppäranta (2015): k_0 increased from -35 W m^{-2} on March 25 to -1 W m^{-2} on May 5. The total modelled surface melting became 36.6 cm, which is rather close to the observation (33 cm) obtained from the ice structure analysis (Table 3). The resulting mean absorption of solar radiation by ice was $Q_A = 5.6$ W m^{-2} corresponding to the melt rate of 0.16 cm d^{-1}, close to 0.18 cm d^{-1} obtained from the ice structure data. To evaluate the heat flux from the water, we took $c = 0.3$ (Leppäranta et al., 2019), and then the contribution of solar radiation to the heat flux to ice bottom became 10.5 W m^{-2}. The background term Q_{w0} is not known but for molecular conduction the scale is $Q_{w0} = k_w \partial T/\partial z \sim 1$ W m^{-2}, where $k_w = 0.56$ W m^{-1} °C^{-1} is thermal conductivity of water, and in general mid-winter data suggest that $Q_{w0} < 5$ W m^{-2}. With $Q_{w0} = 1$ W m^{-2}, we have $Q_w = 11.5$ W m^{-2} and the corresponding melt rate at the ice bottom would be 0.33 cm d^{-1}. This result is supported by the estimate $Q_w = 13$ W m^{-2} from the ice structure data in Section 3.1.

Ice melting obtained from the ice structure data is illustrated in Fig. 6. In 2022, the surface melting was greater than the bottom melting, while in 2018, it was the opposite. The main reason for this difference was in the ice stratification. In 2022, the snow-ice layer accounted for 60 % of the ice cover, while in 2018, the fraction was only 15 %. The melting rate was gradually increasing with the weather getting warmer and solar radiation increasing with time.

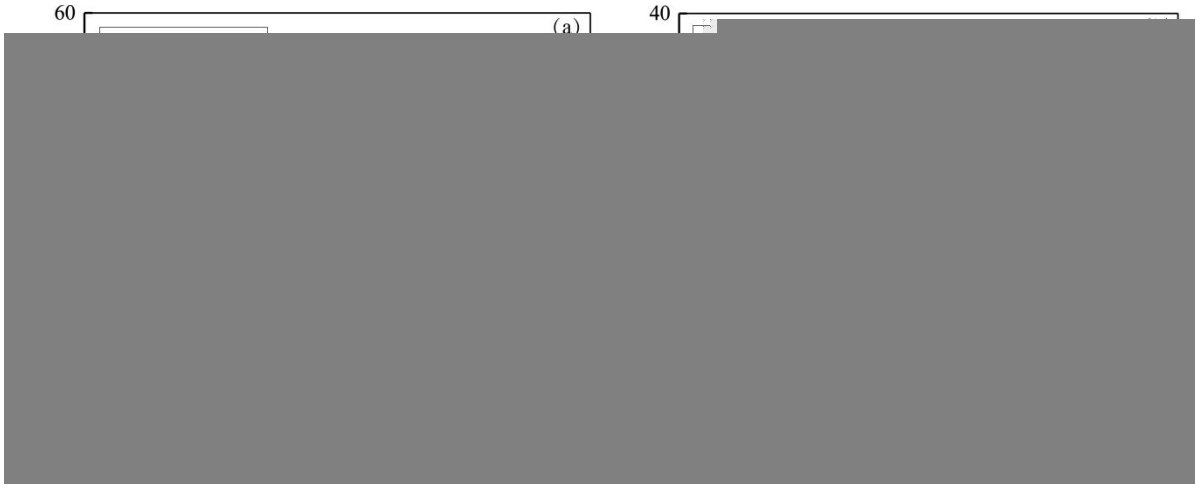

Figure 6. Accumulated ice melting and porosity in 2022 (left) and 2018 (right) based on field data of ice structure. Porosity was not recorded in 2018.

3.4 Ice geochemistry

During the ice decay period, meltwater was mixed into the under-ice water layer that influenced the water geochemistry. In the present data the meltwater had lower pH and EC than the lake water (Figs. 7–8). On April 1, 2022, the mean pH and EC of snow-ice were 6.38 and 17.3 μS cm^{-1}, respectively, and in congelation ice the corresponding values were 6.75 and 9.0 μS cm^{-1}. Atmospheric deposition of acidic substances was judged as the background for the low pH of snow-ice. Then pH and EC decreased. The vertical profiles of EC, pH and Chl *a* show that EC was larger near the snow-ice surface than in congelation ice in the early melting stage, but the difference was no more obvious after April 14. pH was always smaller in snow-ice than in congelation ice. The content of Chl a was less than 0.6 μg L^{-1} with the maximum at the snow-ice–congelation ice interface. In 2018, the limited data showed that EC was 6 μS cm^{-1} and pH was 6.35 in ice.

In lake water, the mean ± standard deviation of pH and EC were 6.82 ± 0.09 and 92.5 ± 12.7 μS cm^{-1}, respectively, in 2022. EC was smaller in ice by one order of magnitude than in water, on average EC(ice) = 0.12·EC(water). EC was decreasing with time in water due to meltwater drainage from ice (Fig. 8). The changes in pH and EC had both signs, caused by flushing by meltwater and lake water. pH increased in the late melting period after the slush layer appeared, likely due to the increase in the

photosynthesis enhanced CO_2 consumption. However, the inflow from brooks into the study bay could cause an opposite effect (Fig. 9). The inflow was weak until April 21, but in April 21–25 it corresponded to 17 % of the water volume of the bay.

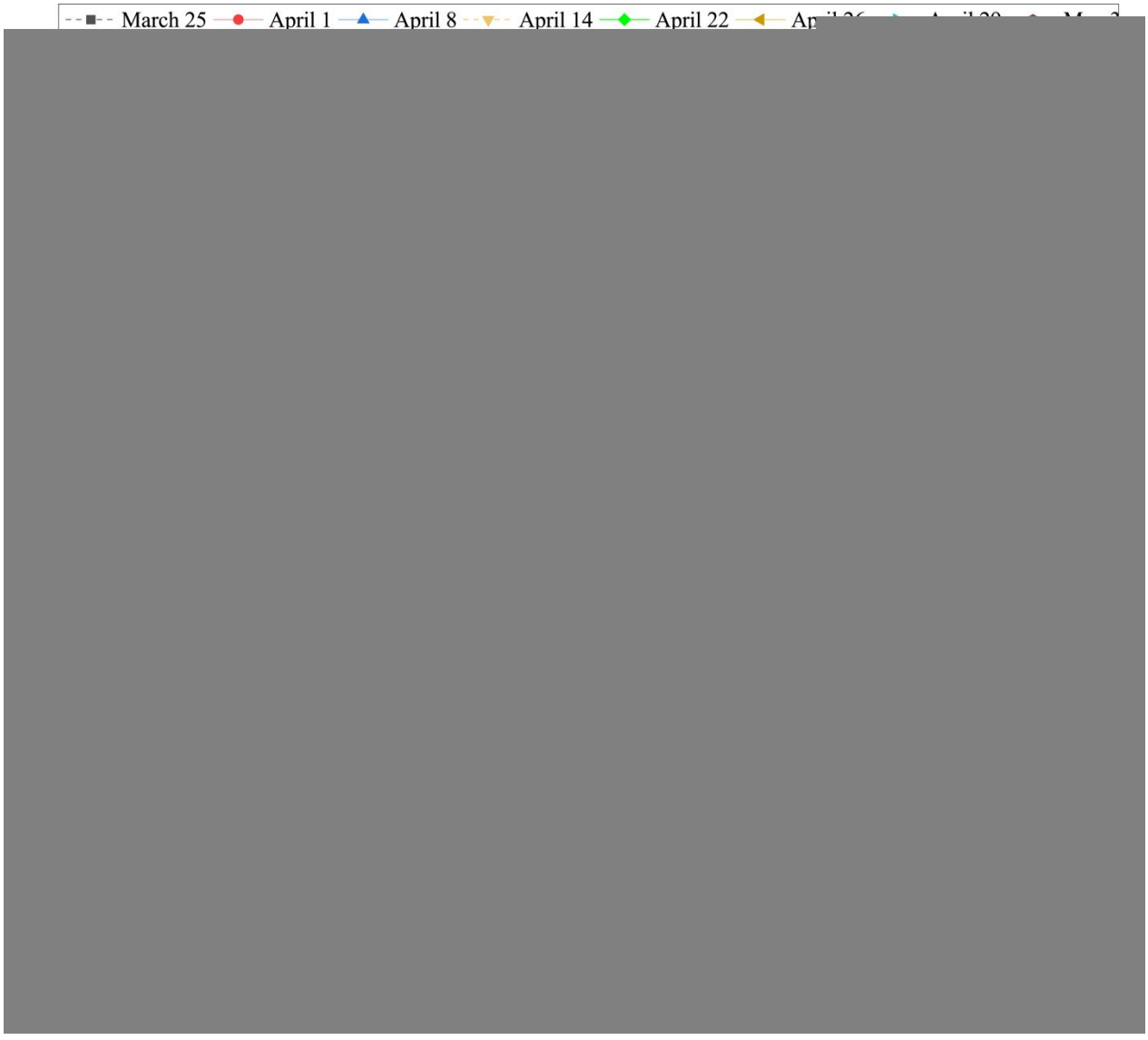

Figure 7. EC, pH and Chl *a* in ice meltwater and under-ice water at the study site in 2022 and 2018. (a) EC in ice meltwater and under-ice water at the study site in 2022; (b) pH in ice meltwater and under-ice water at the study site in 2022; (c) Chl *a* in ice meltwater and under-ice water at the study site in 2022; (d) EC and pH in ice meltwater and under-ice water at the study site in 2018.

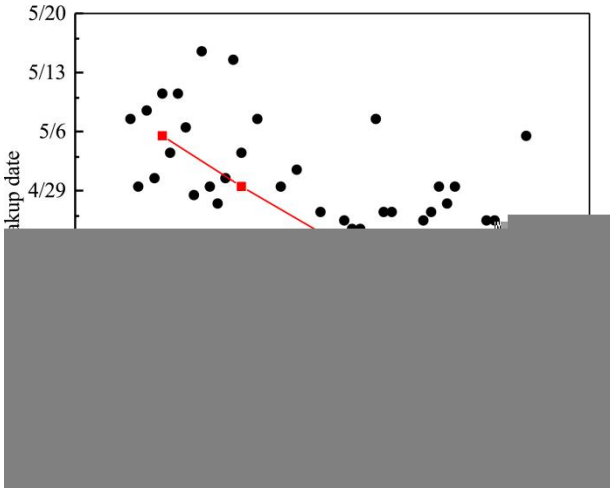

Figure 10. The ice breakup date of Lake Pääjärvi in 1970–2022. The black dots show the breakup date and the red squares show the ice breakup date averaged in every 10 years. Data source: Lammi Biological Station.

4.2 Comparisons of ice melting with other lakes

Melting of ice begins when the heat balance turns positive in spring and takes place at the surface, interior and bottom depending on the ice structure and fluxes. In 2022, the mean melting rate was 0.79 cm d^{-1} at the surface, 0.52 cm d^{-1} at the bottom, and 0.18 cm d^{-1} in the ice interior in Lake Pääjärvi. In an Arctic tundra lake in northern Finland, Lake Kilpisjärvi, the triple (surface, bottom, and internal melting) was (2.9, 0.5, 1.0) cm d^{-1} in a warm spring 2013 and (0.8, 0.1, 1.0) cm d^{-1} in a normal spring 2014 (Leppäranta et al., 2019). In a boreal lake, Lake Vendyurskoe, at 61–62°N, field investigations in two seasons showed the mean melt rates of 1.2 cm d^{-1} at the surface in both cases and 0.8 and 0.2 cm d^{-1} at the bottom (Leppäranta et al., 2010). The differences in the quality of melting are due to differences in the congelation ice/snow-ice fractions and weather conditions that determine the level of light transfer through ice and surface heat balance.

The porosity of ice needs to be estimated to examine the internal melting process. In the present work, the porosity was estimated from the measured ice density directly and from the absorbed solar radiation indirectly. The results were consistent with each other. Increasing porosity during the melting period changes the ice structure and decreases the strength of ice, and finally leads to breakage with rapid final disappearance of ice. Here the breakage took place in May 3–5 when the porosity of the ice

393 was 40 – 50 %. Leppäranta et al. (2019) used the solar radiation method to evaluate the porosity and
394 found the same level at the breakage supporting our result.

395 The heat flux from the lake water body to the bottom of ice has not been much studied (Shirasawa
396 et al., 2006; Kirillin et al., 2012). A heat flux of the order of 1 W m^{-2} represents molecular conduction
397 in the near-surface water layer and may be feasible in mid-winter (e.g., Jakkila et al., 2009; Kirillin et
398 al., 2012; Yang et al., 2012), but in spring, penetration of solar radiation to the water body gives a
399 fractional return flux to the ice bottom. According to the present study, the heat flux from water to ice
400 scales as 10 W m^{-2} in melting period, and the more transparent ice allowed more sunlight penetration
401 and larger heat flux. Jakkila et al. (2009) reported the heat flux values in Lake Pääjärvi as 12 W m^{-2}
during the final stage of ice melting that is very close t

In 2022, the maximum thickness of ice was 55 cm with 60 % snow-ice, and in 42 days the ice melted by 33 cm from the surface and 22 cm from the bottom while the porosity increased from less than 5 % to 40–50 % at breakup. The comparison between ice structure and heat budget gave a good agreement in quantifying the deterioration of the ice cover. This result is promising when considering the possibility of detailed numerical modelling of ice deterioration. The largest uncertainty is in the bottom melting, where more research is needed on under-ice boundary layer dynamics. Solar radiation penetrating through ice adds a major contribution to the heat flux from water to ice, according to the present results on the order of 10 W m^{-2}, which is significantly higher than usually assumed in lake ice modelling.

Ice and water pH and EC decreased during the ice decay but experienced fluctuations due to flushing by meltwater and lake water. The mean EC of ice was 11.4 μS cm^{-1}, equal to the fraction 0.12 of the lake water EC. The mean ice pH was 6.44, lower by 0.4 than in water. Chl *a* in ice increased to 0.6 μg L^{-1} in the late part of ice decay, with the maximum in the slush sub-layer of snow ice. At the end of the decay, Chl *a* was 1.7 μg L^{-1} in water, still far from the first summer maximum.

The results are important for modelling the lake ice season and the annual cycle of lakes. Lake ice has an important role in the physical, chemical, and ecological cycle, and these cycles are sensitive to climate changes. For the ice melting season, detail modelling of the ice strength and the consequent bearing capacity and ice forces has a major importance for the local societies in lake regions.

Data availability. The routine meteorological and hydrological data are available at: https://www.syke.fi and https://www.fmi.fi. The ice samples data applied in this work can be accessed by the link: https://doi.org/10.5281/zenodo.7342770.

Author contributions. YZ conceived the field and laboratory study in 2022 with ML and MF and wrote the paper with contributions from JL and ZL. SS and JA performed the study in 2018. All co-authors discussed the results and edited the manuscript.

Acknowledgements. We are grateful to the Lammi Biological Station and the Institute of Atmospheric and Earth Sciences, University of Helsinki for providing logistical help and laboratories. Thanks to Esa-Pekka Tuominen, Joni Uusitalo and Riitta IIola for helping in the fieldwork and laboratory, and to

Lauri Arvola for comments on the manuscript. This work was financially supported by the National Key Research and Development Program of China (Grant No. 2019YFE0197600), the National Natural Science Foundation of China (Grant No. 52211530038) and the Academy of Finland (350576 and 333889), and a personal grant to Yaodan Zhang by China Scholarship Council (CSC).

Competing interests. The authors declare that they have no conflict of interest.

References

Arst, H., Erm, A., Leppäranta, M., and Reinart, A.: Radiative characteristics of ice-covered freshwater and brackish water bodies, Proc. Estonian Acad. Sci. Geology, 55(1), 3–23, 2006.

Arst, H., Erm, A., Herlevi, A., Kutser, T., Leppäranta, M., Reinart, A., and Virta, J.: Optical properties of boreal lake waters in Finland and Estonia, Boreal Environ. Res., 13, 133–158, 2008.

Arvola, L., Kankaala, P., Tulonen, T., and Ojala, A.: Effects of phosphorus and allochthonous humic matter enrichment on metabolic processes and community structure of plankton in a boreal lake (Lake Pääjärvi), Can. J. Fish. Aquat. Sci., 53, 1646–1662, https://doi.org/10.1139/f96-083, 1996.

Arvola, L., Salonen, K., Keskitalo, J., Tulonen, T., Järvinen, M., and Huotari, J. : Plankton metabolism and sedimentation in a small boreal lake—a long-term perspective, Boreal Environ. Res., 19, 83-96, 2014.

Ashton, G. D.: Deterioration of floating ice covers, J. Energy Resour. Technol.-Trans. ASME, 107, 177–182, https://doi.org/10.1115/1.3231173, 1985.

Ashton, G. D. (Ed.): River and lake ice engineering, Water Resources Publications, Littleton Colorado, 1986.

Benson, B. J., Magnuson, J. J., Jensen, O. P., Card, V. M., Hodgkins, G., Korhonen, J., Livingstone, D. M., Stewart, K. M., Weyhenmeyer, G. A., and Granin N. G.: Extreme events, trends, and variability in Northern Hemisphere lake-ice phenology (1855–2005), Climate Change, 112, 299–323, https://doi.org/10.1007/s10584-011-0212-8, 2012.

Bengtsson, L., and Svensson, T.: Thermal regime of ice covered Swedish lakes, Hydrol. Res., 27, 39–56, 1996.

Bernhardt, J., Engelhardt, C., Kirillin, G., and Matschullat, J.: Lake ice phenology in Berlin–Brandenburg from 1947–2007: observations and model hindcasts, Climatic Change, 112, 791-817, https://doi.org/10.1007/s10584-011-0248-9, 2012.

Cavaliere, E., Baulch, H. M.: Denitrification under lake ice, Biogeochemistry, 137, 285–295, https://doi.org/10.1007/s10533-018-0419-0, 2018.

Deng, Y., Li, Z. K., Li, Z. J., and Wang, J.: The experiment of fracture mechanics characteristics of Yellow River ice, Cold Reg. Sci. Tech., 168, https://doi.org/10.1016/j.coldregions.2019.102896, 2019.

Ellis, A. W., and Johnson, J. J.: Hydroclimatic analysis of snowfall trends associated with the North American Great Lakes, J. Hydrol., 5, 471–486, https://doi.org/10.1175/1525-7541(2004)005<0471:HAOSTA>2.0.CO;2, 2004.

571 Tan, Z., Yao, H. X., and Zhuang, Q. L.: A small temperate lake in the 21st century: Dynamics of water temperature, ice
572 phenology, dissolved oxygen, and chlorophyll a, Water Resour. Res., 54, 4681–4699,
573 https://doi.org/10.1029/2017WR022334, 2018.
574 Vehmaa, A., and Salonen, K.: Development of phytoplankton in Lake Pääjärvi (Finland) during under-ice convective mixing
575 period, Aquat. Ecol., 43, 693–705, https://doi.org/10.1007/s10452-009-9273-4, 2009.
576 Wang, C. X., Shirasawa, K., Leppäranta, M., Ishikawa, M., Huttunen, O., and Takatsuka T.: Solar radiation and ice heat
577 budget during winter 2002–2003 in Lake Pääjärvi, Finland, Verh. Internat. Verein Limnol., 29, 414–417,
578 https://doi.org/10.1080/03680770.2005.11902045, 2005.
579 Warren, S. G.: Optical properties of snow, Rev. Geophys., 20, 67–89, https://doi.org/10.1029/RG020i001p00067, 1982.
580 Williams, G., Layman, K. L. and Stefan, H. G.: Dependence of lake ice covers on climatic, geographic and bathymetric
581 variables, Cold Reg. Sci. Tech., 40, 145–164, https://doi.org/10.1016/j.coldregions.2004.06.010, 2004.
582 Yang, Y., Leppäranta, M., Cheng, B., and Li, Z. J.: Numerical modelling of snow and ice thicknesses in Lake Vanajavesi,
583 Finland, Tellus Ser. A, Dyn. Meteorol. Oceanogr., 64, https://doi.org/10.3402/tellusa.v64i0.17202, 2012.